Contract No F61775-02-WE010: Final Report

Peter V. Sushko, A. Taga, and Alexander L. Shluger*
Department of Physics & Astronomy, University College London, Gower Street, London WC1E 6BT, United Kingdom

I. EXECUTIVE SUMMARY

1. We have developed a new hybrid technique embedding a quantum description of point defects in SiO_2 inside a classical model of the infinite solid. Thus, we incorporate accurately long-range effects (lattice relaxations and dielectric effects). Whilst embedding has been employed previously in highly ionic systems, such as the alkali halides, this is the first successful implementation in a mixed ionic-covalent system. We have demonstrated that many of the geometrical parameters, such as bond lengths and bond angles, are reproduced consistently in both the classical and quantum regions. Furthermore, important quantum mechanical quantities, such as atomic charges and electronic densities of states, show no artifacts due to embedding. Finally, because we are using reliable quantum-mechanical methods, we can calculate excited states with reasonable accuracy and so can study optical properties with a good deal of rigor. This has implications for materials in electronics and for optical fiber materials. While we have chosen one specific material, our work included successful creation of automated techniques for generating force-field parameters in the classical region, as well as pseudopotentials used on frontier pseudo-atoms, so that the method is readily applicable to emerging materials, such as high-K dielectrics.

2. We have applied this new technique to radiation-induced defects in both crystalline and amorphous SiO_2 and developed new insights that change dramatically our understanding of the physics of these centers and hence significantly altered some of the standard models for defect creation in radiation environments such as those found in space. Specifically,

   - The relaxation around the oxygen vacancy is of much longer range than can be captured in current super-cell calculations. This has implications for defect properties in ultra-thin SiO_2 films in MOS devices.
   - We have measured the distributions of structural and spectroscopic properties of oxygen vacancy centers in amorphous silica, that cannot be demonstrated in other calculations.
   - Our modeling predicts the two major structural types of positively charged vacancies (E' centers): dimer and dangling bond centers. The local structure of both types of centers depends on the medium range structure of the surrounding amorphous network. Contrary to the standard model, we find that in amorphous SiO_2 positively charged oxygen vacancies readily distort to localize spin on one side of the defect without one of the silicon atoms rebonding to a three fold oxygen. This implies that E'_γ centers should be much more common that currently thought. For each type of defect we found the distribution of both structural and EPR parameters and calculated optical absorption spectra.
   - We have fully characterized two other structural types of E' centers: the dimer and the back-projected configurations and calculated their spectroscopic parameters.
   - We formulated the structural criteria which favor the formation of different types of center in the original amorphous structure in terms of the average Si–O distance of oxygen ion with its two neighboring silicon ions. This should allow us to estimate the relative concentrations of different defect centers based on the mechanism of their creation.

Thus we have demonstrated that the method has fulfilled many of its promises. It does give greatly improved accuracy over the standard periodic calculations that employ density functional theory for the representation of many important experimentally measured quantities. It has already generated new physical understanding of important radiation-induced defects, indicating its potential importance in the study of emerging materials. The results of this work are presented in the following publications:

1. V. B. Sulimov, P. V. Sushko, A. H. Edwards, A. L. Shluger, and A. M. Stoneham, "Asymmetry and log-range character of lattice deformation by neutral oxygen vacancy in alpha-quartz", *Physical Review B*, **66**, p. 024108, (2002).

2. A. H. Edwards, P. V. Sushko, A. L. Shluger, and V. B. Sulimov, "Embedding techniques for irradiation-induced defects in crystalline and amorphous SiO_2", *IEEE Transactions on Nuclear Science*, **46**(3), pp. 1383-1388, (2002).

3. A. H. Edwards, P. V. Sushko, A. L. Shluger, and V. B. Sulimov, "Embedding techniques for irradiation-induced defects in SiO_2", *6th European Congress on*

REPORT DOCUMENTATION PAGE

Form Approved OMB No. 0704-0188

1. REPORT DATE *(DD-MM-YYYY)*	2. REPORT TYPE	3. DATES COVERED *(From – To)*
22-02-2005	Final Report	5 March 2002 - 05-Mar-03

4. TITLE AND SUBTITLE

New Methodology For First Principle Calculations Of Electrical Levels For Radiation Induced Defects In Silicates

5a. CONTRACT NUMBER
F61775-02-WE010

5b. GRANT NUMBER

5c. PROGRAM ELEMENT NUMBER

6. AUTHOR(S)

Dr. Alexander Shlyuger

5d. PROJECT NUMBER

5d. TASK NUMBER

5e. WORK UNIT NUMBER

7. PERFORMING ORGANIZATION NAME(S) AND ADDRESS(ES)

University College London
Gower Street
London WC1E 6BT
United Kingdom

8. PERFORMING ORGANIZATION REPORT NUMBER

N/A

9. SPONSORING/MONITORING AGENCY NAME(S) AND ADDRESS(ES)

EOARD
PSC 802 BOX 14
FPO 09499-0014

10. SPONSOR/MONITOR'S ACRONYM(S)

11. SPONSOR/MONITOR'S REPORT NUMBER(S)
SPC 02-4010

12. DISTRIBUTION/AVAILABILITY STATEMENT

Approved for public release; distribution is unlimited.

13. SUPPLEMENTARY NOTES

14. ABSTRACT

This report results from a contract tasking University College London as follows: The contractor shall develop a material simulation model and code. This model will be applied to study the geometric and electronic structure, stability and properties of defects in SiO2 dielectrics in semiconductor devices. Specifically, the contractor will deliver:

1. A robust set of force-field, embedding potential (pseudo potential), basis set, shell model that will
a. Reproduce faithfully the lattice parameters for alpha quartz
b. Reproduce faithfully the dielectric constant for SiO2

2. A set of calculations on important intrinsic defects including
a. The oxygen vacancy (in + and o charge states) in both crystalline and amorphous SiO2
b. atomic hydrogen (in + o and - charge states)
c. Self-trapped hole in amorphous SiO2 (model calculations for selected sites)
d. Self-trapped exciton in crystalline SiO2

15. SUBJECT TERMS
EOARD, Semiconductor materials, space materials, Silicon on Insulator (SOI) materials

16. SECURITY CLASSIFICATION OF:			17. LIMITATION OF ABSTRACT	18, NUMBER OF PAGES	19a. NAME OF RESPONSIBLE PERSON
a. REPORT	b. ABSTRACT	c. THIS PAGE			DONALD J SMITH
UNCLAS	UNCLAS	UNCLAS	UL	16	19b. TELEPHONE NUMBER *(Include area code)* +44 (0)20 7514 4953

Radiation and its Effect of Components and Systems, pp. 98-104, (2002).

4. P. V. Sushko, V. B. Sulimov, A. S. Mysovsky, and A. L. Shluger, "Long-range character of lattice distorsion by vacancies in alpha-quartz", *3rd Forum on New Materials - Vol. 1, "Computational Modelling and Simulations of Materials- II"*, pp. 75-86, (2002).

5. A. S. Mysovsky, P. V. Sushko, S. Mukhopadhyay, A. H. Edwards, and A. L. Shluger, "Calibration of embedded cluster method for defect studies in amorphous silica", *Physical Review B*, **69**, p. 085202, (2004).

6. S. Mukhopadhyay, P. V. Sushko, A. H. Edwards, and A. L. Shluger, "Calculation of relative concentration of E' centres in amorphous silica." *Journal of Non-Crystalline Solids*, **345&346**, 703-709, (2004).

7. S. Mukhopadhyay, P. V. Sushko, A. M. Stoneham, and A. L. Shluger, "Modeling of the structure and properties of oxygen vacancies in amorphous silica", *Physical Review B*, **70**, pp. 195203(1-15), (2004).

8. P. V. Sushko and A. L. Shluger, "The effect of the α-quartz lattice on the optical absorption and stretching frequency of the interstitial O2 molecule", *physica status colidi (c)*, **2**(1), pp. 503-506, (2005).

9. S. Mukhopadhyay, P. V. Sushko, V. A. Mashkov, and A. L. Shluger, "Spectroscopic features of dimer and dangling bond E' centres in amorphous silica", *Journal of Physics: Condensed Matter (in press).*

10. S. Mukhopadhyay, P. V. Sushko, A. M. Stoneham, and A. L. Shluger, "Correlation between the atomic structure, formation energies and optical absorption of neutral oxygen vacancies in amorphous silica", *submitted to Physical Review B.*

11. P. V. Sushko, S. Mukhopadhyay, V. B. Sulimov, A. S. Mysovsky, A. L. Shluger, "Structure and properties of defects in amorphous silica: new insights from embedded cluster calculations", *submitted to Journal of Physics: Condensed Matter*

II. INTRODUCTION

Amorphous silica, a-SiO_2, is one of the most technologically important and best studied amorphous materials with a long history of defect studies[1,2]. However, our understanding of the effects of disorder on defect properties and the relative abundance of different defect configurations in amorphous silica is only just starting to develop. Theoretical modeling has been instrumental in developing models of basic defects in silica, starting from pioneering papers by W. B. Fowler *et.al.*[3–7], and has led to significant advances in the field. It has been realized that modeling defects in amorphous materials requires considering not only one or a few sites, as in crystals, but a statistical ensemble of structural sites. The dependence of formation energies, structural parameters, diffusion barriers and spectroscopic parameters of these defects on details of the local and medium range environment should be characterized by some statistical distributions. The structural disorder can also lead to creation of new defect types. Models of these in amorphous materials should take into account the role of local and medium range stress and strain in the surrounding network in defect formation. In a crystal, the defect *model* which comes out of calculations includes a unique set of its main fingerprints, such as the geometric and electronic structure, spectroscopic properties, mechanism of motion (diffusion), reactions with other defects and other parameters which can be studied experimentally and used for ultimate defect identification.

In this project, we have developed an embedded cluster method for predicting and analyzing defect models in a-SiO_2. The purpose of this report is to critically review the scope of this method and to demonstrate its applicability to studying the structure and spectroscopic properties of defects in amorphous silica. Below we consider the basic approaches used in defect studies, describe the embedded cluster method developed within this project and its main advantages with respect to other methods, and present the main results of its application to developing defect models in amorphous silica. The details of the computational scheme are given in Appendix A and the results of the test calculations in Appendix B.

III. MODELING TECHNIQUES

We start from briefly discussing some techniques available for modeling defects in insulators. They exist in the form of computer codes implementing a model of a system with a defect and a method for calculating the defect structure and its properties.

A. Periodic and cluster approaches

Two models are often used in computer simulations of point defects in solids: a *periodic* model, and a finite

cluster model. They differ in the boundary conditions imposed on a system wave-function. Initially, the periodic model was developed for calculation of the electronic structure and properties of ideal crystals, whereas the cluster model was introduced from molecular calculations. However, consequently the terms "periodic model" and "cluster model" for the same defect appeared. It has long been realized that neither of them can be used alone if an accurate picture of a defect is to be established. Therefore, both models were gradually developed to provide accurate descriptions of defect structure and processes.

1. Periodic model

The periodic model is based on a definition of a unit cell (or more generally, a supercell), which can be periodically translated to build an infinite solid as indicated in Fig. 1b and 1c. There are no limitations, in principle, on the size and shape of the unit cell providing that the host lattice is defined unambiguously. Note that the same approach is often used to build models of amorphous solids too. The periodicity imposed on the atomic structure also applies to the electronic structure: the charge density is the same in every supercell and is matched at the boundary between two neighboring supercells. In the case of ideal crystals this approach is technically exact.

To calculate the properties of an individual point defect using the periodic model, a supercell is defined which comprises the defect and its immediate environment (Fig. 1b). The supercell is then periodically repeated as shown in Fig. 1c. The defect in each supercell interacts with an infinite number of similar defects (called images) in all other supercells. Therefore, the application of this approach to individual defects is adequate only if artificial defect-image interaction is small.

One of the most attractive features of the periodic model is that it allows one to consider a perfect system and one with a defect on the same footing. Most of the computer codes implementing the periodic model use a basis set of plane-waves or their variations. This provides a very flexible, potentially complete basis set, a quality almost inaccessible in cluster calculations.

An obvious feature of the periodic model, which can be both to its advantage and disadvantage, is that "defects" are periodically translated and interact between themselves. It can be an advantage if one is interested, for example, in periodic adsorption of molecules at the surface and would like to vary their concentration. It is a drawback if one is interested in the properties of an individual defect in different charge states. In particular, if the defect is charged with respect to the host lattice, the electrostatic interaction of such defects is divergent. Some special techniques developed to deal with this problem are discussed in refs.[8–10]. Yet another downside of the periodic model is that the defect-induced distortion of the host lattice can only be taken into account within the supercell. This may lead to inaccurate results if these distortions propagate further than cell boundaries, but can be checked by increasing the supercell size. Large supercells are required to study complex defects and to account for extended defect-induced lattice deformation. The recently developed "so-called" order-N methods allow one to significantly reduce the computing load by making it just linearly proportional to the number of particles, N, in the system. Supercells including several thousand atoms can be considered using these methods[11,12].

Finally, studying excited states in the periodic model represents a difficult problem. On one hand, excited states are often much more delocalized than the system ground state and hence require much bigger cells for reliable predictions. On the other hand, computational techniques for calculating excited states are less developed in the periodic model compred to those available for molecules and in a cluster model.

To summarize, the periodic model is ideal if one is interested in the ground state properties of neutral defects, which weakly perturb the surrounding lattice.

2. Molecular cluster model

An alternative approach is to consider a point defect and its immediate environment as a large hypothetical molecule usually called a "cluster" (see Fig. 1d). This model is, generally speaking, only applicable if the following two conditions are satisfied: i) the atomic and electronic structure of the host lattice is accurately reproduced by the cluster, and ii) the defect-induced perturbations are essentially localized within the cluster boundaries[13].

To define a cluster means to somehow "cut out" a fragment from an infinitely large host lattice and to consider it separately. The "cutting" could be more easily made by a minimal charge density surface. This is relatively straightforward in atomic, molecular and ionic crystals where structural elements, such as ions or molecules can be well defined and their electron densities separated. As a result, an integer number of molecules or ions can be attributed to a cluster. In the case of polar or covalent crystals the cutting is made through atoms so that the cluster should be terminated by "pseudo-atoms" specially designed to terminate broken bonds (see review[14] for numerous examples).

The range of applications for the cluster model is often complementary to that of the periodic approach. A cluster model is a natural choice if it is essential to consider the properties of an isolated defect in a crystal. Other examples include properties of nano-powders, low-coordinated surface sites or different sites in an amorphous structure, i.e. situations where supercells are difficult to construct or too expensive to consider. One of

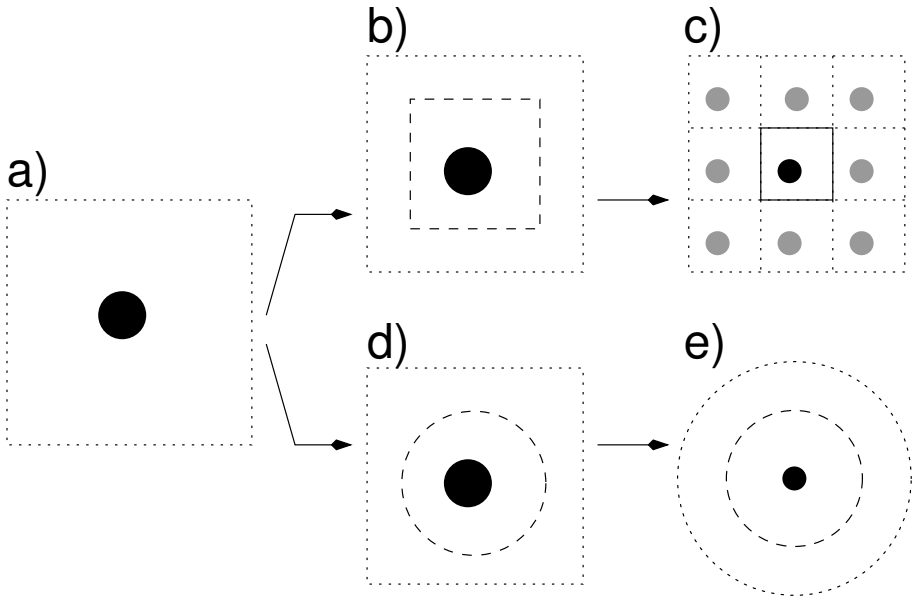

FIG. 1: Periodic and embedded cluster approaches for calculation of point defects in crystals. a) A crystal with a point defect. b) Immediate environment of the defect in the periodic approach is defined as a supercell for periodic calculations. c) The supercell is periodically translated so that to form a new ideal crystal. d) Immediate environment of the defect in the embedded cluster approach is included in a quantum-mechanically (QM) treated cluster. e) The QM cluster is embedded in a classically treated environment (outer circle).

the main advantages of cluster models is the large number of quantum-chemical methods for electronic structure calculations available from molecular calculations, especially for excited states.

On the downside, cluster model calculations are usually more computationally demanding than periodic ones. In spite of enormous advances in computing power, clusters of only a few tens of atoms can be calculated routinely. This is because the computational expense grows as n^4 where n is the number of atomic basis set functions typically used in these calculations.

Using small molecular clusters for treating larger systems brings a number of problems: i) Polarizability of the "surface" ions, especially O^{2-}, is larger than those in the "bulk" of the cluster[15]. A large ratio of "surface" to "bulk" atoms in a small cluster may result in an overestimated electronic polarization due to the "surface" atoms and, in principle, in an incorrect electronic structure altogether. This is manifested in formation of artificial "ghost" states in the band gap. ii) The electrostatic potential due to the host lattice, which is particularly important in ionic compounds, is not adequately treated in small clusters. As a result the positions of energy levels can be wrong. iii) Defect-induced lattice relaxation can be considered only for the atoms nearest to the defect with atoms at the cluster surface usually kept fixed. This implies that the lattice response to the presence of a defect as well as the effect of that response on the defect itself can be significantly underestimated.

In ionic-covalent systems, such as SiO_2, cluster formation always requires breaking chemical bonds. A popular fix in this case is to passivate broken bonds with real hydrogen atoms or with "pseudo"-atoms with parameters specially fitted to fulfil this task. A cluster of $Si_2O_7H_6$ including two tetrahedra connected via a common oxygen atom with all other oxygens passivated by hydrogen atoms is a frequent choice. Note that this cluster is just an artificial construction convenient for studying the local properties of defects in SiO_2.

Thus a molecular cluster model tends to completely disregard the effects of the rest of the atoms outside the cluster and applies some semi-empirical fixes to the atoms at the cluster surface to diminish their adverse effect. This major problem is addressed and partially solved in the *embedded cluster* model.

3. Embedded cluster model

The molecular cluster model can be improved by taking into account the interaction of the quantum cluster with the rest of the host lattice, the perturbation of the lattice by the defect, and the effect of the lattice perturbation on the defect itself. This is achieved by constructing an external potential in which the cluster is then embedded. Such a potential is called an embedding potential and the model, an embedded cluster model. Development of an accurate embedding potential is a major challenge. It aims to "correct" the molecular cluster approach by improving the description of the interaction between the cluster and the rest of the system. This can be done at three levels of sophistication:

- The electrostatic potential due to the part of the crystal lattice outside the cluster is included in the calculations by: i) placing point charges of appropriate value at the lattice sites (see, for example,[16,17]; ii) fitting the Madelung potential by several point charges located at specially selected points; iii) calculating the matrix elements due to the Madelung potential directly and adding these matrix elements to the potential energy matrix[18].

- To further improve the description of the cluster boundary, an interface region between the cluster and the point charges is introduced. Interface atoms can be approximated by effective core pseudo-potentials[19,20] at the cation sites around the cluster or, more accurately by effective potentials calculated self-consistently specifically for the material under study (see, for example, refs.[17,21–23]). The latter approach allows one to reduce the cluster size and the computational load in some cases.

- The defect-induced lattice distortion is accounted for by embedding the cluster in an infinite polarizable lattice of classical ions represented using a shell model[24] or a polarizable ion model[25,26]. Unlike the two previous cases, these ions are not kept fixed, but are allowed to adjust their positions to minimize the total energy of the system. This allows one to relax explicitly a large region (several hundred atoms) of the host lattice near the defect. More importantly, embedding into a polarizable lattice can be done in such a way that it also accounts for the effect of the lattice response on the cluster electronic structure. This allows one to achieve self-consistency in the calculation of the defect-induced lattice perturbation and the effect of this perturbation on the defect structure and properties. This effect is similar in many ways to a polaron digging its potential well in a polarizable media.

Most of the calculations dealing with defects in amorphous silica have so far been made using either periodic or molecular cluster models. In the periodic model, the disorder of the amorphous structure is included explicitly, but within a relatively small periodically translated supercell (see, for example, refs.[27–30]). In the molecular cluster model, a cluster can capture at best the average local structure of the material. A problem pertaining to both models has been that periodic cells and clusters typically include up to 72 atoms, which is hardly enough to consider the medium-range distortion of the amorphous structure induced by the defect. Another important issue concerns the dependence of the results on the quantum mechanical method (see, for example, refs.[31,32]). In particular, as has been demonstrated in refs.[33,34], the electronic structure of polaron and exciton systems depends dramatically on whether Hartree-Fock or Density Functional Theory (DFT) is used. Besides, neither of these two models can be used to build up significant statistics and to find rare precursor sites. The major limitations of periodic DFT calculations relate to predicting narrower band gaps and inability to predict optical absorption and luminescence energies of defects.

The embedded cluster model is designed to overcome the limitations of both models and to allow one to properly treat the defect-induced distortion of amorphous network, build up defect statistics and calculate defect spectroscopic properties with good accuracy. Some examples of the development of this approach and its application to defects in crystalline oxides are discussed in refs.[35–39]. They clearly demonstrate that providing the system is ionic, it can be well treated in the embedded cluster model discussed above. Several embedding schemes have been suggested for treating ionic-covalent systems, such as SiO_2[31,40,41]. They have been successful in predicting ground state properties of crystalline quartz. However, they failed to provide reliable predictions for defect optical absorption energies. This is largely due to the formation of spurious states at the bottom of the conduction band caused by inaccurate treatment of the cluster border within the local embedding potentials approximation[31,35].

To summarize, one of the main advantages of the embedded cluster approach is that it is inherently local by nature and can be easily applied to bulk crystals, amorphous materials, surfaces[42–45] and complex interfaces[46]. However, if building up a quantum cluster requires breaking bonds between atoms, the Coulomb embedding potential is not enough and a more sophisticated treatment is needed. The development of an approach to treating such systems has been at the center of this project.

IV. THE EMBEDDED CLUSTER METHOD IMPLEMENTED IN THE GUESS CODE

The previous generation of the embedded cluster method implemented in the GUESS computer code[39] has been thoroughly described in several recent publications[31,32,43]. Therefore we will only briefly outline the main features of the method and will focus on the details relevant to studying defects in a-SiO_2. The detailed description of the method, typical calculation setups and test calculations are presented in Appendix A and B.

In broad terms, in the embedded cluster method a system, crystalline or amorphous, with a single point defect is divided into several regions. A spherical region I centered at the "site of interest" includes: i) a quantum-mechanically treated cluster (QM cluster), ii) an interface region which connects the QM cluster and the (classical) rest of the solid, and iii) a classical region that surrounds the QM cluster and includes up to several hundred atoms. Region I is surrounded by a finite region II, also treated atomistically and containing up to several thousand atoms. In the course of calculations, all positions of atoms within region I are fully

optimized while atoms in region II remain fixed in the positions corresponding to a perfect crystalline or amorphous structure. Their purpose is to provide the correct electrostatic potential in region I and proper boundary conditions for the atoms at the border of regions I and II. Regions I and II combined together form a finite region which has a radius of several nanometers and is called a *nano-cluster*. Finally, to account for the polarization of the solid from the border between regions I and II and up to infinity, we introduce region III. It is treated in the approximation of a polarizable continuum and conforms geometrically to the boundary between regions I and II.

The whole approach is similar in spirit to the classical Mott-Littleton method[47]. The total energy of the system includes (see Appendix A): i) the energy of the QM cluster and the interface atoms in the external electrostatic potentials due to the classical environment; ii) the interaction between classical atoms in regions I and II calculated using inter-atomic potentials; iii) the short-range interaction of the classical atoms and of the interface atoms with the QM cluster atoms calculated using the short-range part of the classical inter-atomic potentials, and iv) the Mott-Littleton correction for the polarization of region III. This latter correction is about 0.3 eV in the typical setup described below and remains constant in all calculations of singly charged vacancies. The expression for the total energy is given in ref.[31].

The classical atoms in regions I and II are represented using the shell model and the rigid atom model, respectively (see Appendix A). Their electrostatic interaction with the interface and with the QM cluster atoms is included at the quantum-mechanical level, i.e. by calculating the corresponding matrix elements and adding them to the QM potential energy matrix. Total forces are calculated on both QM and classical ions. This allows us to minimize the system total energy simultaneously with respect to the electronic coordinates and the positions of QM ions and classical ions, and hence to avoid the time-consuming "self-consistency" procedure used in some previous implementations of this method[48,49].

Properties of the interface atoms depend on the material in question, as described for MgO[39], SiO_2[31] and Mg_2SiO_4[50]. For SiO_2, a QM cluster is terminated by the Si^* atoms that form an interface between the QM cluster and the rest of the nano-cluster (see Appendix A). The Si^* atoms are located at the Si sites of the SiO_2 structure and represent real Si atoms. This is quite different from many molecular cluster schemes where a QM cluster is terminated by artificial so called pseudo-atoms[51–53]. The Si^* atoms are chosen so that they are coordinated by one quantum-mechanically treated oxygen and three classically treated oxygen ions from the rest of the nano-cluster. They perform a dual role: they form a polar bond with the QM oxygen and describe the interaction with the three classical oxygens. This is achieved by representing Si^* as a combination of $\frac{1}{4}$ of a quantum-mechanical Si atom and $\frac{3}{4}$ of a classical Si atom. The detailed description of Si^* atoms as applied to α-quartz is given in refs[31,32]. The same parametrization scheme is used in the present calculations.

The GUESS code[31,39] plays the role of a "master" program that calculates the total energy, total forces acting on all centers in Region I and performs the geometry optimization of the whole system. Thus the scheme allows us to account consistently for the defect-induced polarization of the host lattice and also the effect of this polarization on the defect itself. The Gaussian 98 package[54] is used for calculations of the quantum mechanical contributions to the total energy and forces.

A. Summary of the new method

The main purpose of this work has been to develop further the embedded cluster method for silica proposed in refs.[31,32,43], and to test it on well-studied defects. We aim to minimize the lattice distortions at the border of a defect-free QM cluster embedded in the classically treated non-defective crystal lattice and to represent the quartz electronic structure as closely as possible to that calculated for the perfect lattice treated periodically. For future calculations of spectroscopic properties, one would like to avoid having spurious electronic states due to the cluster border at the top of the valence band and at the bottom of the conduction band. The scheme developed in this project employs a hybrid density functional similar to the one known as B3LYP which includes the three-parameter Becke's exchange functional[55] and a correlation functional by Lee, Yang, and Parr[56], rather than the Hartree-Fock method used in the earlier studies[31,32]. It makes use of the new semi-local embedding potentials and benefits from improved classical inter-atomic potentials. The latter provide a fully consistent treatment of the crystal surrounding the quantum cluster both in terms of effective ionic charges and the elastic and dielectric properties.

The new generation of the computational embedding technique developed within this project includes several components outlined below and discussed in detail in Appendix A. They are generic to further applications of this method to other systems, such as chalcogenates and high dielectric constant oxides, e.g. HfO_2 and hafnium silicates. The results of test calculations carried out for the non-defective α-quartz lattice and for the structure and spectroscopic properties of the neutral oxygen vacancy in α-quartz are summarized in Appendix B. The results of applying of the new method to studying defect properties in amorphous silica are presented in refs.[31,32,43,57–60].

The computational scheme includes the following components:

First, a periodic calculation of the perfect crystal, α-quartz, is carried out using the CRYSTAL code[61]. This code employs the Gaussian-type basis set and implements the Hartree-Fock method and hybrid density functionals compatible with those implemented in the Gaussian package for quantum-chemical calculations of

molecules[54] and used in further embedded cluster calculations. In periodic calculations we used the 6-31G* basis set and optimized the geometry of the α-quartz lattice including both fractional coordinates and the unit cell parameters.

Second, the parameters of the classical inter-atomic potentials are re-adjusted to reproduce the structure obtained from the periodic calculations and experimental physical properties such as elastic and dielectric constants. The latter are particularly important for accurate calculations of charged defects. The fitted parameters provide consistency of the geometry in the classical region with that within the QM cluster. Changing basis set or functional leads to different geometric parameters of the perfect lattice and may result in artificial strain at the cluster border if the classical interactions are not adjusted accordingly. To efficiently parametrize the classical potentials for the different basis set and/or *ab initio* methods used in the QM calculations, we developed a new computational method which is described in detail in Appendix A. This approach allows us to generate classical potentials that provide an atomic structure consistent with the geometry of the QM cluster and, through this, to minimize the lattice distortions at the interface region in the non-defective system.

Third, the parameters of the interface atoms, Si*, at the border between the QM cluster and the classical region are optimized. These include the parameters of a semi-local pseudo-potential describing the interaction of the border Si* atoms with the electron density in the QM cluster and, effectively, saturating the Si*–O bond directed inside the cluster. This is the vital part of the embedding scheme as it is responsible for eliminating spurious border electronic states and achieving a homogeneous electron density distribution inside the cluster. In addition, there are short-range classical potentials associated with the Si* and its oxygen neighbors. These potentials aim to correct the local atomic structure at the interface. This approach allows us to significantly improve the description of the cluster border (compare, for example, with previous publications by Sulimov *et al.*[31] and Mysovsky *et al.*[32]). In particular, since the parameters of the classical inter-atomic potentials and the effective pseudo-potential for Si* are consistent with the geometry in the QM region, the mismatch in the local atomic structure at the interface is minimized.

Yet another difference between this work and the previous publications has been that we employed the DFT method and a hybrid density functional similar to the B3LYP functional[54] instead of the Hartree-Fock method used before. We adjusted the amount of exact exchange interaction included in this hybrid functional to consider self-trapped holes and to calculate optical absorption energies of point defects in silica in agreement with experiment (see Appendix A). In combination with a Time-dependent DFT scheme for calculating optical transition energies, this led to fairly accurate predictions of the optical transition energies for both neutral and positively charged vacancies as demonstrated in[59,60,62]. This is a considerable improvement with respect to the previous studies which, paves the way to more extensive studies of optical properties of defects in amorphous silica.

To summarize, the developed embedded cluster method allows one: i) To study the full extent of the defect-induced lattice distortion; ii) To consider a fairly large region of the amorphous structure and thus to explore a greater variety of different sites in the amorphous structure and to build more complete statistics of different defect types and configurations. iii) To calculate a wide range of defect properties, including the optical absorption spectra. The experience gained in these calculations and in combining quantum mechanical and classical techniques will be useful for further studies of defects in disordered materials.

V. APPENDIX A: THE EMBEDDED CLUSTER METHOD

In this Appendix we describe in detail the embedding method, the procedure for optimizing the classical shell model inter-atomic potentials and the embedding potential parameters.

A. Calculation of the total energy

In our method the whole system is represented using a large finite nano-cluster of either crystalline or amorphous silica. It uses $\mathrm{Si}(\frac{1}{2}\mathrm{O})_4$ structural elements as building blocks, as described in ref.[43]. The nano-cluster is divided into regions I and II as shown in Fig. 2a. The expression for the total energy is given by:

$$E = E_{QM+IF} + W_{QM+IF,CL} + E_{CL} + E_{ML}, \qquad (1)$$

where E_{QM+IF} is the total energy of the QM cluster and the interface in the electrostatic potential V_{CL}^{Coul} due to the classical environment:

$$V_{CL}^{Coul}(\mathbf{r}) \;=\; \sum_{i}^{N_{cor}} \frac{Q_i^{cor}}{|\mathbf{R}_i^{cor} - \mathbf{r}|} + \sum_{i}^{N_{she}} \frac{Q_i^{she}}{|\mathbf{R}_i^{she} - \mathbf{r}|}.$$

E_{QM+IF} also includes a classical term $W_{IF,QM}^{S-r}$, which describes a non-Coulombic interaction between the interface and QM cluster atoms; it is a correction to the electronic pseudo-potentials $\hat{V}_i$ centred on the interface atoms. Similarly, the classical term $W_{QM+IF,CL}^{S-r}$ describes the non-Coulombic short-range interaction between the classical atoms and atoms of the QM cluster and the interface. E_{CL} is the total energy of the classical environment and E_{ML} is the Mott-Littleton polarization energy of the lattice outside region I.

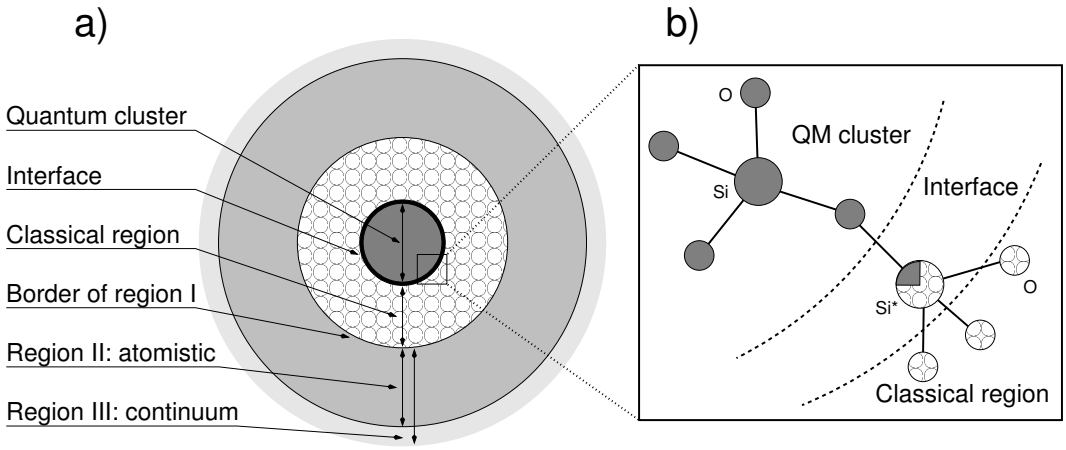

FIG. 2: a) General setup for the embedded cluster calculations: the division of the whole system into sub-regions is shown. b) Schematic description of the interface between the quantum-mechanically treated cluster and classical environment.

In more detail:

$$E_{QM+IF} = \langle\Phi|H_0 + W^{Coul}_{CL,QM+IF}|\Phi\rangle + W^{S-r}_{IF,QM}, \quad (2)$$

where

$$\begin{aligned} H_0 \;=\; & -\sum_i^{N_e}\frac{1}{2}\nabla_i^2 - \sum_i^{N_{QM+IF}}\sum_j^{N_e}\frac{Z_i}{|\mathbf{R}_i-\mathbf{r}_j|} \\ & + \sum_{i<j}^{N_e}\frac{1}{|\mathbf{r}_i-\mathbf{r}_j|} + \sum_{i<j}^{N_{QM+IF}}\frac{Z_iZ_j}{|\mathbf{R}_i-\mathbf{R}_j|} + \sum_i^{N_{IF}}\hat{V}_i \end{aligned}$$

$$W^{Coul}_{CL,QM+IF} \;=\; \sum_i^{N_e} V^{Coul}_{CL}(\mathbf{r}_i) + \sum_j^{N_{QM+IF}} V^{Coul}_{CL}(\mathbf{R}_i)$$

$$W^{S-r}_{IF,QM} = \sum_i^{N_{QM}}\sum_j^{N_{IF}} U_{ij}(\mathbf{R}_i-\mathbf{R}_j)$$

The total energy of the classical region is given by

$$\begin{aligned} E_{CL} \;=\; & \sum_i^{N_{CL}}\frac{k_i}{2}|\mathbf{R}_i^{cor}-\mathbf{R}_i^{she}|^2 + \sum_{i<j}^{N_{CL}} U_{ij}(\mathbf{R}_i-\mathbf{R}_j) \\ & + \sum_{i<j}^{N_{cor}+N_{she}}\frac{Q_iQ_j}{|\mathbf{R}_i-\mathbf{R}_j|}, \end{aligned}$$

$$W^{S-r}_{CL,QM+IF} = \sum_i^{N_{QM+IF}}\sum_j^{N_{CL}} U_{ij}(\mathbf{R}_i-\mathbf{R}_j),$$

and

$$E_{ML} = -\frac{1}{2}Q^2\left(\sum_i\sum_{\alpha\beta=1}^{3}\frac{M_i^{\alpha\beta}r_i^\alpha r_i^\beta}{r_i^6}\right)$$

In the expressions above N_{QM+IF} is the total number of atoms in both the QM cluster and at the interface together, whilst N_e stands for the total number of electrons shared between them. N_{CL} is the total number of classical atoms, and N_{cor} and N_{she} are the total numbers of classical cores and shells respectively. Z are the charges of nuclei in the QM cluster and at the interface, Q^{cor} and Q^{she} are charges of the classical cores and shells. $\mathbf{R}^{cor}$ and $\mathbf{R}^{she}$ are the coordinates of the classical cores and shells. The Hamiltonian H_0 includes the kinetic energy of the electrons, the electrostatic interaction of the electrons and the nuclei in the QM cluster and the interface, and effective pseudo-potentials for the interface atoms. Terms $W^{S-r}_{CL,QM+IF}$ and $W^{S-r}_{IF,QM}$ can be represented by pair-wise Buckingham or Morse-type classical potentials U_{ij}, defined for each pair of atoms i and j, as well as 3- and 4-body classical potentials. Constants k are related to polarizability of ions. The Mott-Littleton correction E_{ML} is calculated over a region which conforms geometrically to the boundary of region I and extends to infinity. The constants $M_i^{\alpha\beta}$ represent on-site polarizabilities, Q is the net charge of the defect with respect of the lattice, and r_i is the distance from each atoms to the centre of region I[63].

The quantum-mechanical contributions to the total energy and forces are calculated using the Gaussian 98 package[54] for *ab initio* calculations of molecules. Details of the parametrization of the interface Si* for silica are considered in more detail below in section V B 3.

B. Optimizing the embedding parameters

The scheme described above requires an adequate choice of the *ab initio* method and basis set for the QM cluster and of the inter-atomic potentials for the classical atoms in regions I and II. These should be consistent with the properties of the interface atoms at the border between the QM cluster and the classical region. In this section we describe our approach to the parametrizing these components of the scheme.

1. Classical potentials

Several sets of classical inter-atomic potentials for silica have been previously developed. However, these potentials do not fully satisfy our needs for two reasons. Firstly, we wish to achieve consistency between the atomic structure of the QM cluster and that of the classical region. In other words, the classical potentials should provide the same cell parameters and fractional coordinates as those obtained from a reference quantum-mechanical calculation. In our case the reference calculation is carried out using the CRYSTAL code and Gaussian-type basis set. Secondly, to the best of our knowledge, classical potentials with non-formal charges on Si and O ions[64,65] fail to reproduce the static dielectric constant of α-quartz and that of amorphous SiO_2.

Since the atomic structure obtained in these calculations will depend on the basis set and the *ab initio* technique, a method for fast re-optimization of the classical potentials is needed. This method has been developed on the basis of an existing package MERLIN[66] for minimization of functionals in multi-dimensional space.

In the following we describe the details of the reference CRYSTAL calculation used in this work, the details of the re-optimization procedure, and, finally, compare the performance of the classical potentials found in this work against those reported previously.

The primitive unit cell of α-quartz is defined by six parameters: two of them (a and c) determine the size of the unit cell and the remaining four (u, x, y and z) determine the fractional coordinates of Si and O atoms. The total energy of α-quartz was minimized with respect to these six parameters using the periodic model and the CRYSTAL code. Standard 6-31G* basis sets on Si and O atoms and the hybrid B3LYP density functional[61] were employed in these calculations. The energy minimization was done in two steps. First, the fractional coordinates were fully relaxed for the fixed lattice parameters a and c. Then the fractional coordinates were fixed and a and c were relaxed manually. Then both steps were repeated until overall convergence was achieved. The total energy per unit cell was converged within 10^{-6} eV, the lattice cell vectors within 0.0005 Å and the fractional coordinates within 0.0005. The structure of α-quartz obtained here is in agreement with the results of previous calculations[67]. In particular, we found that a=4.933 Å and c=5.402 Å.

TABLE I: Parameters of the classical inter-atomic potential optimized for α-quartz. A, ρ and C are the Buckingham potential parameters for the interaction between Si–O and O–O ions. k is the spring constant for the interaction between O core and shell. The Si charge is $2.4|e|$, O core charge is $-1.619|e|$, and O shell charge is $0.419|e|$.

	A (eV)	ρ (Å)	C (eV·Å^6)	k (eV/Å^2)
Si–O	3185.06	0.24102	46.72	
O–O	7682.67	0.25627	0.01	16.6

To optimize the parameters of the inter-atomic potentials, $\mathbf{p} = (p_1, p_2, .., p_n)$, we have defined a cost function

$$F(\mathbf{p}, \mathbf{f}^0, \mathbf{f}) = \sum_i w_i \cdot (f_i^0 - f_i(\mathbf{p}))^2,$$

where $\mathbf{f} = (f_1, f_2, ..)$ define numerical values of the properties to be fitted to the corresponding set $\mathbf{f}^0$ of the reference values. Weights w_i were set to 80.0 for the geometrical parameters of the unit cell and to 2.0 for the elastic and the dielectric constants. Reference geometrical parameters in $\mathbf{f}^0$ were taken from the reference CRYSTAL calculation while the elastic and dielectric constants were taken from experimental data.

The optimization of parameters $\mathbf{p}$ was carried out using the MERLIN optimization package[66] which implements a modification of the "Controlled Random Search" (CRS) technique originally introduced by Price[68]. To calculate the value of the cost function for each probe set of parameters $\mathbf{p}$, we use the GULP code (General Utility Lattice Program)[63] which relaxes the α-quartz lattice using the inter-atomic potentials supplied by the MERLIN search engine and then calculates the physical properties at the equilibrium configuration. After that the cost function for the given probe set of parameters is calculated and supplied back to the search engine. In this way, all the parameters of the classical potentials for Si–O and O–O interaction, as well as the spring constants and charges of the O shells can be fitted simultaneously. Thus this approach provides a flexible, yet efficient tool for a general minimization problem able to cope with very complex landscapes.

To fit the parameters for the inter-atomic potentials we first set the total ionic charges on Si and O ions to $2.4|e|$ and $-1.2|e|$ respectively and defined upper and lower limits for all other parameters. The potentials generated using the MERLIN code are summarized in Table I.

The properties of α-quartz calculated using the parameters obtained in this work are compared with experimental data in Table II. The same set of properties was calculated using other 2-body potentials reported previously. The BKS potentials[65] were modified so that the rigid ion model for oxygen ions was replaced by the polarizable ion model[43]. The original potentials reported by SMC[69] also contain a corrective 3-body term; the re-

TABLE II: Comparison of several parameter sets for α-quartz. a and c are the hexagonal lattice parameters in Å, B is the bulk modulus in GPa units, c_{ij} are the elastic tensor components in 10 GPa units, ϵ^0_{11} and ϵ^0_{33} are the static dielectric constants, and ϵ_∞ is the high frequency dielectric constant.

	experiment	this work	BKS[1]	TTAM[2]	SMC[3]
a	4.916	4.931	4.933	5.041	4.849
c	5.405	5.404	5.432	5.552	5.401
b	37	37.8	41.8	32.5	-
C_{11}	8.69	8.87	9.14	7.25	6.20
C_{13}	1.19	0.95	1.73	1.13	1.63
C_{14}	-1.81	-1.60	-1.72	-1.49	-1.01
C_{33}	10.50	10.51	11.13	8.71	7.44
C_{44}	5.28	5.63	5.09	3.94	3.30
C_{66}	3.99	3.90	4.07	3.23	2.74
ϵ^0_{11}	4.52	4.41	1.96	2.09	5.51
ϵ^0_{33}	4.46	4.55	2.01	2.15	6.09
ϵ_∞	2.4	2.40	1.54	-	2.06
Ionic charges					
Si		2.4	2.4	2.4	4.0
O		-1.2	-1.2	-1.2	-2.0

[1] from ref.[65]
[2] from ref.[64]
[3] from ref.[69]

sults presented in Table II have been calculated without the 3-body correction.

We note that, as well as a generally better agreement with the experimental data, the potentials obtained in this work reproduce well the reference geometry, for which they were fitted and the dielectric constants. The latter, as we discussed above, is essential for an accurate calculation of the long-range lattice polarization induced by charged defects.

2. The density functional

It is a well-established fact that different quantum-mechanical methods can produce qualitatively different results. For example, plane-wave DFT calculations with PW91 functional do not reproduce the electronic structure of the V_K centre in NaCl[34], a prototype hole center well-studied experimentally. This has been attributed to the inaccurate treatment of the exchange interaction in the PW91 density functional[70]. On the other hand, calculations made with the Hartree-Fock approach do include the exact exchange E^{HF}_{ex} but suffer from the lack of the electron correlation. A way forward was suggested in the form of hybrid density functionals, which contain an admixture of E^{HF}_{ex}. For example, there is 20% of E^{HF}_{ex} in the B3LYP[55] and 50% in the BH&H[71] density functionals. However, depending on the system and/or class of problems, the amount of E^{HF}_{ex} that needs to be included in the calculations may vary. A possible strategy is to include the parametrization of the E^{HF}_{ex} admixture that fits best for a given problem.

We illustrate this idea with the example of optical absorption of the neutral vacancy in α-quartz. We form a BxLYP density functional and vary the E^{HF}_{ex} contribution so as to reproduce the optical absorption spectrum of the Si_2H_6 molecule[72]. This molecule has been previously considered as a model for the neutral vacancy in α-quartz.

We found that the main features of the Si_2H_6 absorption spectrum were reasonably well reproduced if the B3LYP functional and a standard 6-31G basis set were used. However, with a more flexible basis set aug-cc-pVTZ[54], the absorption maxima shifted to lower energies. When the amount of E^{HF}_{ex} was increased from 20% to 32.5%, the agreement between the experimental and theoretical spectra improved if the same aug-cc-pVTZ basis set was used. In the following calculations (see Section VI) we use this modified BxLYP functional.

A similar fitting approach can be used when, for example, properties of self- trapped holes in a-SiO_2 or excitons are studied. In these cases the amount of the E^{HF}_{ex} will, generally speaking, be different.

3. The interface Si* atoms

In the present embedded cluster calculations of SiO_2, a QM cluster is terminated by Si* atoms that form an interface between the QM cluster and the rest of the system. The Si* atoms are located at the Si sites of the SiO_2 structure and represent real Si atoms. This is in contrast to many other molecular cluster schemes where a QM cluster is terminated by artificial so-called pseudo-atoms located in the middle of Si–O bonds[51–53,73–75].

The Si* atoms are chosen so that they are coordinated by one quantum-mechanically treated oxygen and three classically treated oxygen ions. The dual role of Si* atoms is to interact quantum-mechanically with their QM neighbors, i.e. to form a polar bond with QM oxygen atoms, and interact classically with classical oxygens. This is achieved by representing Si* as a combination of $\frac{1}{4}$ of a quantum-mechanical Si atom and $\frac{3}{4}$ of a classical Si atom.

The detailed description of such a division is given in refs. 31,32. Briefly, Si* is an one-electron atom; its interaction with the rest of the system is defined by several parameters which are: i) the nucleus charge of Si* related to the effective ionic charge of silicon in SiO_2, ii) the effective core pseudo-potential $\hat{V}_i(\mathbf{r})$, iii) the atomic basis set, and iv) the classical short-range inter-atomic potentials that describe the interaction of the Si* with its neighbors in the QM cluster and in the classical environment. These components are inter-related and, therefore, should be fitted together.

The meaning of the first two components of the Si* parametrization can be highlighted as follows. For a

given ionic charge Q_{Si} for Si ions in SiO_2 the amount of the electron charge donated to each neighboring O is calculated as $\frac{1}{4}Q_{Si}$. Therefore, Si*, as an one-electron atom with only one quantum-mechanically treated neighbor, should have a nuclear charge equal to $1 + \frac{3}{4}Q_{Si}$. This provides a deep potential well for the electrons, which has to be locally compensated by a short-range Effective Core Pseudo-potential (ECP) to reproduce the effect of the core electrons in real Si atoms. The atomic Gaussian-type basis set of Si* consists of a single s basis function that corresponds to the valence shell of the 6-31G basis set for Si atoms.

In the current parametrization we employed a semi-local pseudo-potential, which is better suited for describing the directed Si–O bond than the local pseudo-potential used in the previous parametrization. The analytical form of this pseudo-potential is that of Hay and Wadt[19]:

$$\hat{V}(\mathbf{r}) = U_L(r) + \sum_{l=0}^{L-1}[U_l(r) - U_L(r)|\hat{P}_l\rangle\langle\hat{P}_l|,$$

where $|\hat{P}_l\rangle\langle\hat{P}_l|$ is the projector on the basis functions of the orbital momentum l.

In this project we developed the Si* ECP with $L = 1$. Functions $U_l(r)$ were expanded over 10 primitive functions of the form: $Ce^{-\alpha r^2}r^{2-n}$ where C are expansion coefficients and $n = 0, 1, 2$.

To fit the potential we fixed the powers of n_i and varied parameters C_i and α_i in two steps. First, the effective potential for Si* was fitted on the Hartree-Fock level for the $Si_2O_7Si^*_6$ QM cluster in the ideal α-quartz configuration. In these calculations we demanded that the distribution of the electron density, as given by the Natural Population Analysis (NPA), inside the QM cluster was homogeneous and the direction and the electronic structure of Si*–O bonds, as given by Natural Bonding Analysis (NBA), were similar to those calculated for real Si–O bonds. Moreover, the average charges of the three types of ions should be balanced. This can be expressed by the following equations:

$$Q_{Si} = -2Q_O = 4Q_{Si^*}$$

In addition, we demand that the energy of the localized electronic hole (h^+) should be independent of whether the hole is localized on the oxygen ion at the centre of the QM cluster or at its boundary. The energy of the hole was calculated as the difference between the total energies of the ground and ionized states. A similar criterion was used for the localized unrelaxed excitons where we demanded that the excitation energies, calculated via Singlet–Triplet transitions ($S \rightarrow T$), were independent of the exciton localization site.

The optimized set of parameters C_i, α_i and n_i provided $E(h^+_{centre})$ =14.93 eV and $E(h^+_{periphery})$ =14.92 eV. Similarly, $E(S \rightarrow T)_{centre} = 10.06$ eV and $E(S \rightarrow T)_{periphery} =$ 9.57 eV were calculated. These results indicate that the effective pseudo-potential developed for Si* in this work provides a reasonably accurate embedding potential with an expected error of about 0.5 eV for the excitation energies close to the inter-band transitions.

In the second step of the Si* ECP optimization, the radial functions $U_l(r)$ obtained above were scaled with coefficients β and γ so that $C'_i = \beta C_i$ and $\alpha'_i = \gamma\alpha_i$, where β and γ were varied independently for each $U_l(r)$ to satisfy the same criterion on the homogeneous distribution of the electron density as described above. The geometrical parameters, e.g. Si–O inter-atomic distances, inside the QM cluster should were also required not to depend on the distance from the center of the bond to the boundary of the cluster. To achieve this, parameters β and γ for each $U_l(r)$ were scaled independently to minimize cost-functions associated with the above conditions. The MERLIN package was used for these calculations in the same spirit as described above in section V B 1.

Finally, the classical interaction of the interface Si* atoms with other lattice atoms was calculated as follows. The pair-wise interaction of Si* with classical atoms was taken to be the same as the Si–O interaction in the classically treated part of the system. The Si*–O bond with the QM oxygen was simulated using a Morse-type potential $V(r) = D_e\left[\left(1 - e^{-\alpha(r-r_0)}\right)^2 - 1\right]$ with parameters D_e=28 eV, α=3.9 Å^{-1}, and r_0=1.59 Å. In addition to the pair-wise interactions, classical three-body potentials of the form $\frac{k}{2}(\theta-\theta_0)^2$ were introduced at the interface between the QM cluster and the classical region to correct for the distortion of Si*–O–Si angles. The force constant of k=4 eV/rad^2 was fitted for these potentials.

At the end of the total energy minimization with respect to the coordinates of all centers in region I, we found that the local geometry of the QM cluster was very close to the ideal α-quartz structure (see Table III). The largest deviation of an O atomic charge from the corresponding average was smaller than 0.02 $|e|$ and the ratio of calculated average atomic charges on Si, O, and Si* atoms was 3.98:–1.98:1, i.e. very close to the ideal ratio of 4:–2:1. Details of the *perfect lattice test* calculations for QM clusters $Si_2O_7Si^*_6$ and $Si_8O_{25}Si^*_{18}$ are described in the next section.

VI. APPENDIX B: TEST CALCULATIONS

To test the performance of the new method and to illustrate the significance of different components of the embedding potential, we consider two types of problems. First, to demonstrate improved consistency between the quantum-mechanically and classically treated regions, we study the electronic and geometric structures of the perfect α-quartz lattice as a function of the cluster size and compare the results with the periodic CRYSTAL calculations as well as with the results obtained using an earlier parametrization for SiO_2 based on a local effec-

TABLE III: Average geometrical parameters in the QM cluster and at the interface (Si–O and Si*–O distances, Si–O–Si and Si*–O–Si angles) and NPA atomic charges used to characterise the quality of embedding in V_{s-loc}-scheme, V_{s-loc}-scheme, and H-scheme. Ratio Q(Si):Q(O′):Q(Si*) is calculated with respect to the Q(Si*). E_{gap} is the difference between the highest occupied and the lowest unoccupied one-electron states. The notations are described in the text. Distances, angles, and the atomic charges are given in Å, degrees and $|e|$ respectively. E_{gap} is given in eV. Numbers in brackets indicate the range of the corresponding values (from their maximum to minimum).

Property	This work				Earlier scheme[31]				Free clusters			
	$Si_2O_7Si^*_6$		$Si_8O_{25}Si^*_{18}$		$Si_2O_7Si^*_6$		$Si_8O_{25}Si^*_{18}$		$Si_2O_7H_6$		$Si_8O_{25}H_{18}$	
Si–O	1.635	(0.022)	1.638	(0.042)	1.608	(0.043)	1.617	(0.068)	1.688	(0.015)	1.680	(0.034)
Si*–O	1.636	(0.002)	1.636	(0.002)	1.554	(0.002)	1.554	(0.002)	0.966	(0.008)	0.965	(0.013)
Si–O–Si	146.1	(n/a)	145.0	(3.9)	147.7	(n/a)	148.1	(6.2)	146.8	(n/a)	148.3	(12.2)
Si*–O–Si	142.5	(1.9)	142.3	(2.6)	149.1	(1.6)	147.8	(3.6)	131.1	(11.6)	128.7	(16.4)
Q(Si)	2.51	(0.00)	2.52	(0.03)	2.61	(0.01)	2.59	(0.04)	2.42	(0.01)	2.45	(0.12)
Q(O′)	–1.27	(n/a)	–1.27	(0.01)	–1.22	(n/a)	–1.25	(0.03)	–1.28	(n/a)	–1.28	(0.01)
Q(O″)	–1.25	(0.01)	–1.25	(0.01)	–1.41	(0.01)	–1.41	(0.01)	–1.13	(0.02)	–1.12	(0.03)
Q(Si*) / Q(H)	0.63	(0.01)	0.63	(0.01)	0.74	(0.01)	0.74	(0.01)	0.53	(0.01)	0.53	(0.02)
Q(Si:O′:Si*)	3.98:–2.02:1		4.00:–2.02:1		3.53:–1.65:1		3.50:–1.69:1		4.57:–2.42:1		4.62:–2.40:1	
E_{gap}	9.34		8.71		7.50		7.04		10.17		9.44	

tive pseudo-potential[31] (V_{loc}-scheme), and a traditional scheme where hydrogen atoms are used to terminate the dangling bonds (H-scheme). Second, the ground state structure and optical properties of the neutral oxygen vacancy in α-quartz are calculated using the scheme presented above and compared with the results obtained both V_{loc}-scheme and H-scheme.

The general setup for the embedded cluster calculations has been described previously in[31,32,43]. Here we use a spherical nano-cluster of radius of 30 Å built of $Si(\frac{1}{2}O)_4$ building blocks. Region I, where all atoms were fully relaxed, contained the same number of atoms (789) in both calculations of the non-defective lattice and of oxygen vacancies. In the free cluster calculations the terminating hydrogen atoms were fixed at a distance of 0.98 Å from their oxygen neighbours so that the directions of O–H bonds coincided with the directions of the equivalent O–Si bonds in α-quartz and all other atoms were fully relaxed. Three QM clusters were used: $Si_2O_7Si^*_6$, $Si_8O_{25}Si^*_{18}$, and $Si_{21}O_{56}Si^*_{28}$, where Si* is an interface atom in the case of embedded cluster calculations or a hydrogen atom in the case of the H-scheme.

The standard 6-31G basis set was used for all QM atoms unless otherwise stated. The hybrid BxLYP functional containing the Lee, Yang and Parr correlation[56] and modified Becke three-parameter exchange functional[55] with 32.5% Hartree-Fock exchange was used. The optical absorption energies were calculated using the Time-Dependent DFT (TDDFT) as implemented in the Gaussian 98 code[54]

A. Perfect lattice

To assess the quality of the embedded cluster scheme we have measured several characteristics listed in Table III. The geometry of the QM cluster after the full energy minimization can be described using: i) average Si–O bond length and average Si–O–Si angle inside the QM cluster, ii) average Si*–O bond length at the interface, and iii) average Si*–O–Si angle at the QM cluster border. To characterise the distribution of the electron density inside the QM cluster one can use NPA atomic charges averaged over: i) all Si atoms in the QM cluster (Q(Si)), ii) O atoms (denoted as O′) that are coordinated by two QM Si atoms in the QM cluster (Q(O′)), iii) O atoms (denoted as O″) that are coordinated by one Si* and QM Si atoms (Q(O″)), and iv) all Si* atoms (Q(Si*)). Finally, one can compare the ratio of the atomic charges Q(Si):Q(O′):Q(Si*) with the "ideal" ratio of $4 : -2 : 1$.

A comparative analysis of the data collected in Table III suggests that the scheme presented in this work provides a substantial improvement over the earlier scheme reported in ref. 31. In particular, the mismatch between Si–O and Si*–O inter-atomic distances has been removed and the spread of the geometrical parameters has become smaller. More importantly, however, the distribution of the electron density, as manifested by the atomic charges, is more homogeneous in the present scheme and the ratio of charges is closer to the stoichiometry of the system. For example, atomic charges on oxygens coordinated by two QM Si atoms and by a QM Si and interface Si* atoms are almost identical, in contrast to the earlier V_{loc} scheme. In addition, the one-electron band gap is now closer to the experimental value of 9.65 eV as determined by EELS[77]. The traditional H-scheme results in a much less accurate atomic structure

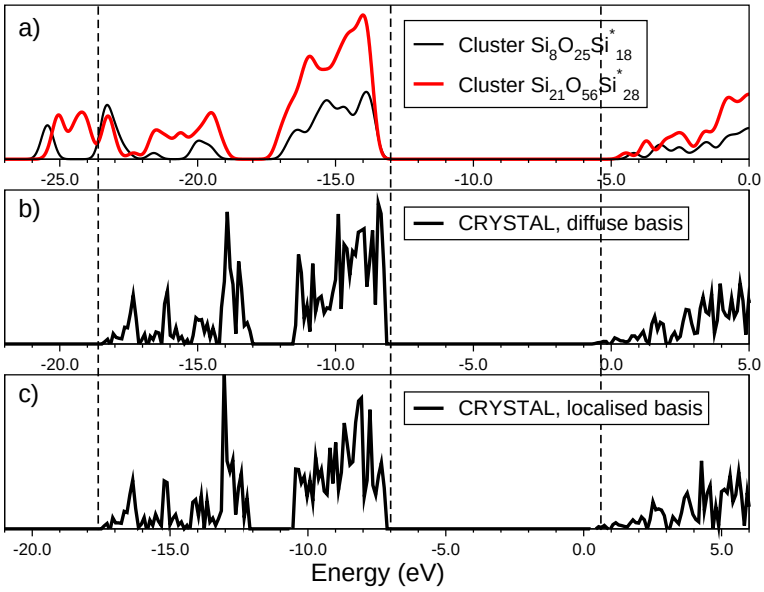

FIG. 3: Densities of states calculated for α-quartz structure using the embedded cluster and periodic approaches. a) embedded cluster DOS calculated using 6-31G basis set[76] (bas_{G98}); b) periodic model DOS calculated using the same basis bas_{G98}; c) periodic model DOS calculated using a more localized basis developed for CRYSTAL calculations[61] (bas_{C03})

with the spread of Si–O–Si angles as large as 12° and an inhomogeneous charge density.

To demonstrate the dependence of the density of states (DOS) on the cluster size we compare the DOS calculated using the current V_{s-loc}-scheme for two QM clusters (Fig. 3a) and that calculated using the periodic model and the CRYSTAL-03 code (Figs. 3b and 3c). For the sake of comparison we used the same geometrical parameters in all three calculations.

The DOS in Fig. 3a was calculated using the embedded cluster approach for QM clusters $Si_8O_{25}Si^*_{18}$ (black) and $Si_{21}O_{56}Si^*_{28}$ (red) and a standard 6-31G basis set for molecular calculations (bas_{G98} thereafter)[76]. The DOS in Fig. 3b was calculated using the periodic model and the CRYSTAL-03 code and the same bas_{G98} basis set. Finally, Fig. 3c shows the DOS calculated with the same periodic model and the basis optimized for bulk calculations of SiO_2 crystal (bas_{C03}). Vertical dashed lines indicate the boundaries of the valence and conduction bands. The energy axes were shifted so that the top of the valence band coincides in all three cases.

The positions of the top of the valence band and the bandgap obtained in the two embedded cluster calculations are identical in both calculations. The profiles of the upper part of the valence band (between –17 eV and –13 eV in Fig. 3a are also very similar. In fact, the only difference appears to be in the profiles of the lower part of the valence band (from –26 eV to –20 eV) formed by the Si–O bonding states. Analysis of these states suggests that the state associated with Si*–O bonds at the interface are shifted to lower energies (from –26 to –23 eV) than the equivalent states at the center of the cluster (from –23 to –19 eV). This shift is due to the semi-local effective potential defined for interface Si* atoms which "drives" the VB states to lower energies. Since the relative number of interface Si*–O in $Si_{21}O_{56}Si^*_{28}$ cluster is smaller than in $Si_8O_{25}Si^*_{18}$ cluster, the DOS in the lower energy part of the valence band for the former is more accurate and shows better agreement with the DOS obtained in periodic calculations. Finally we note the results of the periodic calculations are virtually identical for the basis sets bas_{G98} and bas_{C03}.

We conclude that the band gap and the main features of the Density of State obtained in the embedded cluster calculations agree well with the DOS obtained in periodic calculation with the exception of the Si*–O bond states at the cluster interfaces. The profile of the upper VB remains almost unaffected by the cluster size thus indicating that the nature of the lone pairs is well reproduced in relatively small clusters. In other words, the main features of the density of states are determined by the interactions between the nearest Si and O ions however the valence band width and fine features of the DOS depend on the cluster size and the quality of embedding.

TABLE IV: Properties of the neutral oxygen vacancy in α-quartz. Average Si–Si distances, position of the vacancy level above the Valence Band for the unrelaxed (u) and relaxed (r) vacancies, unrelaxed and relaxed vacancy formation energies and optical absorption energies and oscillator strengths.

Properties		This work		Earlier scheme[31]		Free clusters	
		$Si_2O_7Si_6^*$	$Si_8O_{25}Si_{18}^*$	$Si_2O_7Si_6^*$	$Si_8O_{25}Si_{18}^*$	$Si_2O_7H_6$	$Si_8O_{25}H_{18}$
Ground state							
Si–Si	(r)	2.375	2.404	2.383	2.398	2.568	2.398
$\epsilon_{vac} - \epsilon_{VB}$	(u)	2.55	2.47	2.60	2.84	2.67	2.10
$\epsilon_{vac} - \epsilon_{VB}$	(r)	0.60	0.49	0.68	0.63	0.72	0.34
ϵ_{vac} shift		1.95	1.98	1.92	2.21	1.95	1.76
E_{form}	(u)	7.96	7.81	7.94	8.04	7.82	7.83
E_{form}	(r)	6.20	6.18	6.33	6.27	6.78	6.34
E_{relax}		1.76	1.63	1.61	1.77	1.04	1.49
Optical transitions							
$\sigma \to \sigma^*$	(r)	7.42(0.19)	7.59(0.44)	5.24(0.15)		6.20(0.25)	7.15(0.40)
$\sigma \to \pi$	(r)	7.87(0.08)	7.70(0.19)	5.86(0.04)		7.29(0.08)	7.36(0.05)
$\sigma \to \pi$	(r)	8.05(0.09)	7.81(0.08)	6.18(0.06)		7.73(0.04)	7.62(0.08)

B. Properties of the neutral oxygen vacancy in α-quartz

The properties of the neutral oxygen vacancy calculated using the three computational schemes are summarized in Table IV.

The neutral oxygen vacancy (NOV) in α-quartz is present in the form of a Si–Si bond formed by two Si atoms after an oxygen atom, occupying the site between them, has been removed. It is convenient to characterize the geometric structure of NOV using the distance between the two Si atoms. Formation of the Si–Si bond induces a strong relaxation of the lattice around the vacancy[31]. Calculations made using both embedding schemes and large H-terminated clusters result in almost identical Si–Si bond lengths. Clearly, the Si–Si bond is under-relaxed if only a few atoms near the vacancy are allowed to relax as is the case for small H-terminated clusters.

An accurate account of the NOV-induced lattice relaxation is essential since it affects the formation energy of a defect differently to its electronic properties. For example, all three schemes suggest that the un-relaxed NOV formation energy is between 7.8 and 8.0 eV. After relaxation both embedding schemes give the formation energy as between 6.2 and 6.3 eV regardless of the size of the QM cluster, while in the H-terminated scheme the formation energy is 6.3 eV for the larger cluster and 6.8 eV for the smaller one. The calculated relaxation energies suggest that even in the case of the large H-terminated QM cluster the NOV is not fully relaxed, since the corresponding relaxation energy of 1.5 eV is slightly larger then the 1.6–1.8 eV relaxation for the embedding schemes. At the same time, all the computation schemes considered agree on the position of the one-electron level ϵ_{vac} of the unrelaxed vacancy and put it at about 2.5–2.8 eV above the top of the Valence Band ϵ_{VB}. This level shifts down by aproximately the same value (1.95–2.2 eV) once the lattice relaxation is taken into account.

The optical transitions calculated for NOV have three major contributions. The most intensive transition corresponds to an excitation from the occupied σ state of the vacancy to the unoccupied σ^* state (see Fig. 4a). Two other transitions can be characterized as $\sigma \to \pi$ transitions (Fig. 4b). The σ^* and two π states are induced by the vacancy and their one-electron energies split slightly from the bottom of the Conduction Band. The full optical absorption spectrum also contains transitions from the Valence Band states to the unoccupied states induced by the vacancy and from the occupied σ state to the Conduction Band. These transitions, however, have much smaller oscillator strengths.

The excitation energies and the oscillator strengths calculated for the most intensive transitions are summarized at the end of Table IV. It is immediately clear that the excitation energies are greatly underestimated if the calculations are carried out using the Si* parametrization reported in[31]. This is not surprising since that parametrization was based on ground state calculations only. The excitation energies obtained using the current parametrization are in line with experimentally observed optical absorption of NOV at 7.6 eV. An extensive discussion on the optical absorption of NOVs in amorphous silica can be found in[60]. Finally, in the case of the small H-terminated free cluster $Si_2O_7Si_6^*$ the transition energies are underestimated with respect to the experiment. As the cluster is increased, the excitation energies become larger and closer to the expermental data. This effect is attributed to an insufficiently accurate electrostatic potential at the vacancy site and its environment

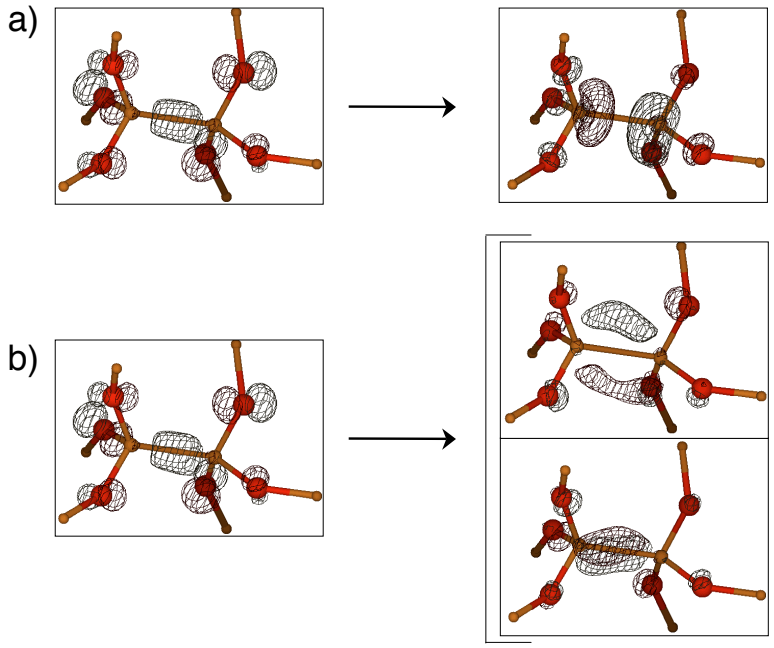

FIG. 4: The most active optical transitions for the neutral oxygen vacancy in α-quartz. a) $\sigma \rightarrow \sigma^*$ transition; b) two $\sigma \rightarrow \pi$ transitions.

in the case of the free clusters. Clearly, this potential is taken into account in the embedded cluster calculations.

* Corresponding author: a.shluger@ucl.ac.uk

[1] G. Pacchioni, L. Skuja, and D. L. Griscom, eds., *Defects in SiO_2 and Related Dielectrics: Science and Technology*, NATO Science Series, Series II: Mathematical and Physical Chemistry (Kluwer Academic Publishers, Dordrecht, 2000).

[2] R. A. B. Devine, J.-P. Duraud, and E. Dooryhée, eds., *Structure and Imperfections in Amorphous and Crystalline Silicon Dioxide* (John Wiley & Sons, Ltd., 2000).

[3] K. L. Yip and W. B. Fowler, Phys. Rev. B **11**, 2327 (1974).

[4] F. J. Feigl, W. B. Fowler, and K. L. Yip, Solid State Commun. **14**, 225 (1974).

[5] A. H. Edwards and W. B. Fowler, J. Phys. Chem. Solids **46**, 841 (1985).

[6] J. K. Rudra and W. B. Fowler, Phys. Rev. B **35**, 8223 (1987).

[7] K. C. Snyder and W. B. Fowler, Phys. Rev. B **48**, 13238 (1993).

[8] G. Makov and M. C. Payne, Phys. Rev. B **51**, 4014 (1995).

[9] L. N. Kantorovich, Phys. Rev. B **60**, 15476 (1999).

[10] P. A. Schultz, Phys. Rev. Lett. **84**, 1942 (1999).

[11] J. M. Soler, E. Artacho, J. D. Gale, A. García, J. Junquera, P. Ordejón, and D. Sánchez-Portal, J. Phys.: Condens. Matter **14**, 2745 (2002).

[12] D. R. Bowler, T. Miyazaki, and M. J. Gillan, J. Phys.: Condens. Matter **14**, 2781 (2002).

[13] G. Pacchioni, P. S. Bagus, and F. Parmigiani, eds., *Cluster models for surface and bulk phenomena* (Plenum Press, New York, 1992).

[14] J. Sauer, Chem. Rev. **89**, 199 (1989).

[15] P. W. Fowler and P. A. Madden, J. Phys. Chem. **89**, 2581 (1985).

[16] N. C. Bacalis and A. B. Kunz, Phys. Rev. B **32**, 4857 (1985).

[17] Z. Barandiarán and L. Seijo, J. Chem. Phys. **89**, 5739 (1988).

[18] K. Todnem, K. J. Børve, and M. Nygren, Surf. Sci. **421**, 296 (1999).

[19] P. J. Hay and W. R. Wadt, J. Chem. Phys. **82**, 270 (1985).

[20] W. R. Wadt and P. J. Hay, J. Chem. Phys. **82**, 284 (1985).

[21] I. V. Abarenkov, V. L. Bulatov, R. Godby, V. Heine, M. C. Payne, P. V. Souchko, A. V. Titov, and I. I. Tupitsyn, Phys. Rev. B **56**, 1743 (1997).

[22] N. Govind, Y. A. Wang, and E. A. Carter, J. Chem. Phys. (1999).

[23] L. Seijo and Z. Barandiaran, J. Chem. Phys. **121**, 6698 (2004).

[24] B. G. Dick and A. W. Overhauser, Phys. Rev. **112**, 90 (1958).

[25] A. Aguado, L. Bernasconi, and P. A. Madden, Chem. Phys. Lett. **356**, 437 (2002).

[26] C. Domene, P. W. Fowler, P. A. Madden, J. J. Xu, R. J.

Wheatley, and M. Wilson, J. Phys. Chem. A **105**, 4136 (2001).
[27] A. Bongiorno and A. Pasquarello, Phys. Rev. Lett. **88**, 125901 (2002).
[28] M. Boero, A. Pasquarello, J. Sarnthein, and R. Car, Phys. Rev. Lett. **78**, 887 (1997).
[29] D. Donadio, M. Bernasconi, and M. Boero, Phys. Rev. Lett. **87**, 195504 (2001).
[30] Z.-Y. Lu, C. J. Nicklaw, D. M. Fleetwood, R. D. Schrimpf, and S. T. Pantelides, Phys. Rev. Lett. **89**, 285505 (2002).
[31] V. B. Sulimov, P. V. Sushko, A. H. Edwards, A. L. Shluger, and A. M. Stoneham, Phys. Rev. B **66**, 024108 (2002).
[32] A. S. Mysovsky, P. V. Sushko, S. Mukhopadhyay, A. H. Edwards, and A. L. Shluger, Phys. Rev. B **69**, 085202 (2004).
[33] G. Pacchioni, F. Frigoli, D. Ricci, and J. A. Weil, Phys. Rev. B **63**, 054102 (2001).
[34] J. L. Gavartin, P. V. Sushko, and A. L. Shluger, Phys. Rev. B **67**, 035108 (2003).
[35] R. Pandey and J. M. Vail, J. Phys.: Condens. Matter **1**, 2801 (1989).
[36] J. M. Vail, J. Phys. Chem. Solids **51**, 589 (1990).
[37] C. Sousa and F. Illas, J. Chem. Phys. **115**, 1435 (2001).
[38] H. Donnerberg and A. Birkholz, J. Phys.: Condens. Matter **12** (2000).
[39] P. V. Sushko, A. L. Shluger, and C. R. A. Catlow, Surf. Sci. **450**, 153 (2000).
[40] V. A. Nasluzov, E. A. Ivanova, A. M. Shor, G. N. Vayssilov, U. Birkenheuer, and N. Rösch, J. Phys. Chem. B **107**, 2228 (2003).
[41] P. Sherwood, A. H. de Vries, M. F. Guest, G. Schreckenbach, C. R. A. Catlow, S. A. French, A. A. Sokol, S. T. Bromley, W. Thiel, A. J. Turner, et al., J. Mol. Struct. - Theochem **632**, 1 (2003).
[42] P. V.Sushko, A. L. Shluger, K. Hayashi, M. Hirano, and H. Hosono, Phys. Rev. Lett. **91**, 126401 (2003).
[43] S. Mukhopadhyay, P. V. Sushko, A. M. Stoneham, and A. L. Shluger, Phys. Rev. B **70**, 195203 (2004).
[44] P. V. Sushko, A. L. Shluger, and C. R. A. Catlow, Surf. Sci. **450**, 153 (2000).
[45] P. V. Sushko, J. L. Gavartin, and A. L. Shluger, J. Phys. Chem. B **106**, 2269 (2002).
[46] M. A. Johnson, E. V. Stefanovich, and T. N. Truong, J. Phys. Chem. B **102**, 6391 (1998).
[47] N. F. Mott and M. J. Littleton, Trans. Faraday Soc. **34**, 485 (1938).
[48] A. L. Shluger, E. A. Kotomin, and L. N. Kantorovich, J. Phys. C: Solid State **19**, 4183 (1986).
[49] A. L. Shluger and J. D. Gale, Phys. Rev. B **54**, 962 (1996).
[50] J. S. Braithwaite, P. V. Sushko, K. Wright, and C. R. A. Catlow, J. Chem. Phys. **116**, 2628 (2002).
[51] G. Pacchioni, G. Ieranò, and A. M. Márquez, Phys. Rev. Lett. **81**, 377 (1998).
[52] D. Erbetta, D. Ricci, and G. Pacchioni, J. Chem. Phys. **113**, 10744 (2000).
[53] T. Uchino, M. Takahashi, and T. Yoko, Phys. Rev. Lett. **86**, 5522 (2001).
[54] M. J. Frisch, G. W. Trucks, H. B. Schlegel, G. E. Scuseria, M. A. Robb, J. R. Cheeseman, V. G. Zakrzewski, J. J. A. Montgomery, R. E. Stratmann, J. C. Burant, et al., *GAUSSIAN 98 (Revision A.7)*, Gaussian Inc., Pittsburgh PA, USA (1998).
[55] A. D. Becke, J. Chem. Phys. **98**, 5648 (1993).
[56] C. Lee, W. Yang, and R. G. Parr, Phys. Rev. B **37**, 785 (1988).
[57] A. H. Edwards, P. V. Sushko, A. L. Shluger, and V. B. Sulimov, IEEE Trans. on Nucl. Sci. **49**, 1383 (2002).
[58] S. Mukhopadhyay, P. V. Sushko, A. H. Edwards, and A. L. Shluger, J. Non-Cryst. Solids **345&346**, 703 (2004).
[59] S. Mukhopadhyay, P. V. Sushko, V. A. Mashkov, and A. L. Shluger, J. Phys.: Condens. Matter (in press).
[60] S. Mukhopadhyay, P. V. Sushko, A. M. Stoneham, and A. L. Shluger, submitted to Phys. Rev. B (2004).
[61] V. R. Saunders, R. Dovesi, C. Roetti, R. Orlando, C. M. Zicovich-Wilson, N. M. Harrison, K. Doll, B. Civalleri, I. Bush, P. D'Arco, et al., *CRYSTAL2003 User's Manual*, Torino (2003).
[62] A. Taga, P. V. Sushko, A. S. Mysovsky, and A. L. Shluger, to be published.
[63] J. D. Gale and A. L. Rohl, Molec. Simul. **29**, 291 (2003).
[64] S. Tsuneyuki, M. Tsukada, H. Aoki, and Y. Matsui, Phys. Rev. Lett. **61**, 869 (1988).
[65] B. W. H. van Beest, G. J. Kramer, and R. A. van Santen, Phys. Rev. Lett. **64**, 1955 (1990).
[66] D. G. Papageorgiou, I. N. Demetropolous, and I. E. Lagaris, Comput. Phys. Commun. **109**, 227 (1998).
[67] B. Civalleri, C. M. Zicovich-Wilson, P. Ugliengo, V. R. Saunders, and R. Dovesi, Chem. Phys. Lett. **292**, 394 (1998).
[68] W. L. Price, in *Towards Global Optimisation*, edited by L. C. W. Dixon and G. P. Szeö (North Holland Publishing Company, 1978), vol. 2, pp. 93–101.
[69] M. J. Sanders, M. Leslie, and C. R. A. Catlow, J. Chem. Soc., Chem. Commun. pp. 1271–1273 (1984).
[70] J. P. Perdew and Y. Wang, Phys. Rev. B **46**, 12947 (1992).
[71] A. D. Becke, J. Chem. Phys. **98**, 1372 (1993).
[72] U. Itoh, Y. Toyoshima, H. Onuki, N. Washida, and T. Ibuki, J. Chem. Phys. **85**, 4867 (1986).
[73] M. J. Field, P. A. Bash, and M. Karplus, J. Comput. Chem. **11**, 700 (1990).
[74] K. P. Eurenius, D. C. Chatfield, B. R. Brooks, and M. Hodoscek, Int. J. Quantum Chem. **60**, 1189 (1996).
[75] D. Das, K. P. Eurenius, E. M. Billings, P. Sherwood, D. C. Chatfield, M. Hodošček, and B. R. Brooks, J. Chem. Phys. **117**, 10534 (2002).
[76] M. J. Frisch, G. W. Trucks, H. B. Schlegel, G. E. Scuseria, M. A. Robb, J. R. Cheeseman, J. J. A. Montgomery, T. Vreven, K. N. Kudin, J. C. Burant, et al., *GAUSSIAN 03 (Revision B.04)*, Gaussian Inc., Pittsburgh PA, USA (2003).
[77] L. A. J. Garvie, P. Rez, j. R. alvarez, P. R. Buseck, A. J. Craven, and R. Brydson, American Mineralogist **85**, 732 (2000).